Zirconia-Based Powders Produced by Plasma-Spray Pyrolisys and Properties of Sintered Ceramics

S N Kulkov[1], S Buyakova[1], L A Gömze[2]

[1]Institute of Strength Physics and Materials Science SB RAS, Tomsk, Russia
National research Tomsk State University, avenue Lenin, 36, 634050, Tomsk, Russia
[2]Department of Ceramics and Silicate Engineering, University of Miskolc, Miskolc, Hungary

E-mail: kulkov@ms.tsc.ru

Abstract. It have been studied zirconia-based powders and sintered ceramic. It was shown that in the porous structure of zirconia-based ceramics there is a critical value of porosity the material divides into two sub-systems, being variously deformable under external loading. It have been shown that *m*-phase in ZrO_2 is formed due to increase in the microdistortion level which destabilizes the nanocrystalline *t* phase. It has been found out the correlation between the sizes of crystallites and porosity, which associated with transition of the isolated porous structure to the continuous one and the porosity of 20%, corresponds to the first percolation threshold.

1. Introduction

Nanocrystalline powders obtained by plasma-chemistry methods are a promising material for production of zirconia-based ceramics. Powders of this sort exhibit a more uniform constituent element distribution over particles as compared to those prepared by conventional processes [1], and a larger amount of excess energy is stored in these powders than in their coarse-grained cousins. In this connection, an investigation of the structure and phase composition in the powders and sintered materials under consideration assumes particular importance, because it extends the possibilities to generate a necessary structure of the materials.

It is known that materials with a stochastic pore structure are attracting great interest because of their wide application as filters for fluid purification and separation, catalyst carriers, heat-insulating coatings, etc. [2]. Ceramic materials have high chemical and corrosion resistance and, therefore, have advantages over metals and high-molecular compounds when used in an aggressive environment or at elevated temperatures. Most ceramics are chemically inactive in biological media, so that associated porous products can be implanted into the human organism (bone tissue endoprotheses and medicinal preparation dispensers).

The synthesis of porous materials with desired property call for the detailed investigation of a correlation between the physics-mechanical properties of the material and its structure. This is especially true for ceramic materials, because porosity, as a rule, leads to a catastrophic decreasing of the strength. Porous ceramics are a heterogeneous material. Depending on its applications, the pore size and the porosity may vary in a very wide range. Therefore, their mechanical behavior is also of scientific interest.

Zirconia is among the materials that are promising for porous structures. It has high strength, fracture toughness, and corrosion resistance. Also, zirconia is stable in aggressive media and does not react with human organism tissues. This ceramic, containing a controllable pore concentration, retains strength properties due to transformation toughening [3].

The aim of this work is to study changes in the features of the structure and phase composition of nanocrystalline zirconia-based powders and the effect of pore morphology on the mechanical behavior of partially stabilized zirconia subjected to high compressive deformation.

2. Materials and Experimental Technique

We have studied powders produced by plasma spray synthesis of nitrate salts of Zr, Y, and Al in a high-frequency discharge. During the experiments, a drop of the aqueous solution used turned into a solid powder particle (within < 1s) that cooled down very quickly. The powders were of the following chemical composition: ZrO_2 + 3 mol % Y_2O_3 (ZrO_2 (3Y), called a binary system), and ZrO_2 (3Y) + 20 wt % Al_2O_3 (ZrO_2 (ZrO_2 (3Y) + 20 wt % Al_2O_3, called a ternary system).

X-ray analysis was performed by means of a DRON-UM1 diffractometer with filtered CuK_a or FeK_a radiation. Point-by-point measurements were taken with a step of 0.1 or 0.05^0. X-ray diffraction lines of the tetragonal phase were indexed on the basis of a face-centered tetragonal unit cell. The lattice parameters were determined from all reflections at angles lying in the range $20 < 2\theta < 120$. Overlapping x-ray diffraction peaks were separated by means of a computer code based on a minimum deviation of the total approximation profile from the experimental one. The phase abundances in the zirconia powder were calculated from the integrated line intensity ratio for the tetragonal (111) and monoclinic ($\bar{1}$ 11) and (111) phases, using a standard formula [6]. The phase composition was calculated to within 5 %.The lattice strains and coherently diffracting domain (CDD) size were found from x-ray line broadening (FWHM). The contributions associated with the effects of microdistortions and range of crystallite dimensions were separated by the approximation method, using the Cauchy-type functions. The physical broadening β served as a basis for construction of a plot on the $(\beta\cos\theta/\lambda)$–$(\sin\theta/\lambda)$ coordinates. The slope $4\langle\varepsilon\rangle$ and the quantity $1/D$ plotted and extrapolated on the ordinate (ε is the rms lattice microdistortions and D is the CDD average size) were estimated by the least-squares technique [4]. Coarse-grained α-quartz was used as a standard for determining the instrumental broadening.

The grain structure was examined under a transmission electron microscope (TESLA BS-500) at an accelerating voltage of 90 kV, using carbon replicas or foils. The latter were obtained by ion-beam milling of thin powder-compact plates.

The porosity of ceramic samples ranged between 2 and 70%, and the mean pore size was comparable to or much larger (by several orders of magnitude) than the grain size. The samples were prepared by the power metallurgy method (pressing with the subsequent sintering of the ultra-fine powder at temperatures of 1200-1600°C). In this way, samples with a pore size comparable to the grain size were obtained. Larger pores were produced by adding granulated admixtures that are easy to burn out, such as rosin or paraffin, into the powder. Compression tests were carried out on an INSTRON-1185 machine with a constant loading rate of $3\text{x}10^{-4}$ s^{-1}. From stress-strain curves, it have been evaluated the strain and the ultimate strength of the material.

3. Results and Discussion

3.1. Electron microscopy of the structure of powders produced by plasma spray synthesis

Data obtained by transmission electron microscopy (TEM) show that the morphology of the ZrO_2 (3Y) powder particles is typical for plasma spray synthesis. The major fraction of the particles is hollow spheres, semispheres or films. Figure 1 shows typical electron micrographs of ZrO_2 (3Y) and ZrO_2 (3Y) + 20wt. % Al_2O_3 powders. The particles are seen to be polycrystals, with their electron diffraction patterns having a ring structure typical for the nanocrystalline state. The system of the Debye rings seen in the electron diffraction patterns of the majority of particles corresponds to high-temperature tetragonal (*t*) or cubic (*c*) ZrO_2 modifications. Moreover, reflections of the monoclinic (*m*) zirconia modification are observed in the electron diffraction patterns of the structure characterized by larger grains. Dark-field microscopy of the nanostructure of zirconia powder particles suggests that the major fraction of crystallites of size $D < 50$ nm is single-domain particles. X-ray spectral microanalysis of individual powder particles shows no difference in Y_2O_3 concentration between particles made up of coarse and fine crystallites. The average amount of Y_2O_3 is ~ 3 mol %, with the standard deviation of the Y_2O_3 content for different powder particles being ≤ 1 mol %. This implies no correlation between the occurrence of the *m* modification and the changing composition. More likely the reflections of *m*-ZrO_2 seen in the electron diffraction patterns of coarse-grained particles suggest a crystallite size of several tens of nanometers for the powder under study. In the case where the crystallite size is above the critical value, the *m* modification is formed. According to the data obtained from dark-field microscopy, up to three defocusing levels of polycrystalline

structure images are revealed for the majority of particles. This bears witness to a multiple-grain layered structure of the particles.

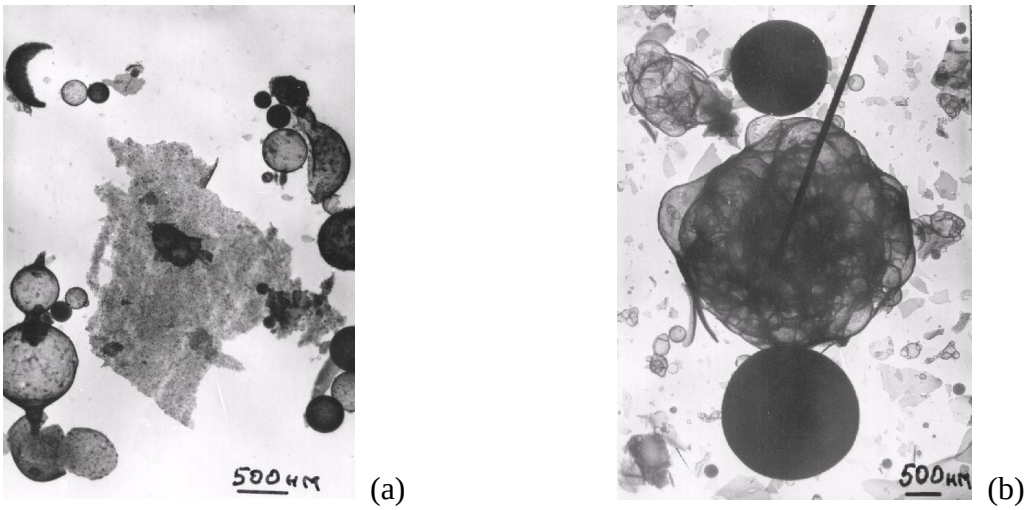

(a) (b)

Figure 1. Typical electron micrographs of ZrO_2 (3Y) (a) and ZrO_2 (3Y) + 20 wt. % Al_2O_3 (*b*)

Figure 2 shows the crystallite particle size distribution among nanocrystalline particles in the powders under review transparent to the incident electron beam. The average crystallite size for ZrO_2 (3Y) powder is 20 nm (Fig. 2*a*), approaching an average size of 22 nm found in other zirconia powders produced by plasma spray synthesis [5,6]. ZrO_2 (3Y) powder exhibits a "broad" crystallite size distribution with variance $\sigma = 11.1$. The largest crystallite size ($D > 30$ nm) may run into 80 nm. However, their contribution is moderate (≤ 10 %). The zirconia crystallite size distribution in the nanocrystalline particles of ZrO_2 (3Y) + 20 % Al_2O_3 is illustrated in Fig.2*b*. The structure of the transparent powder particles under study is seen to consist of smaller grains than those found in the binary system. The average zirconia crystallite size revealed by dark-field microscopy in the (111) reflection of high-temperature ZrO_2 phases is 9 nm with $\sigma = 5.2$.

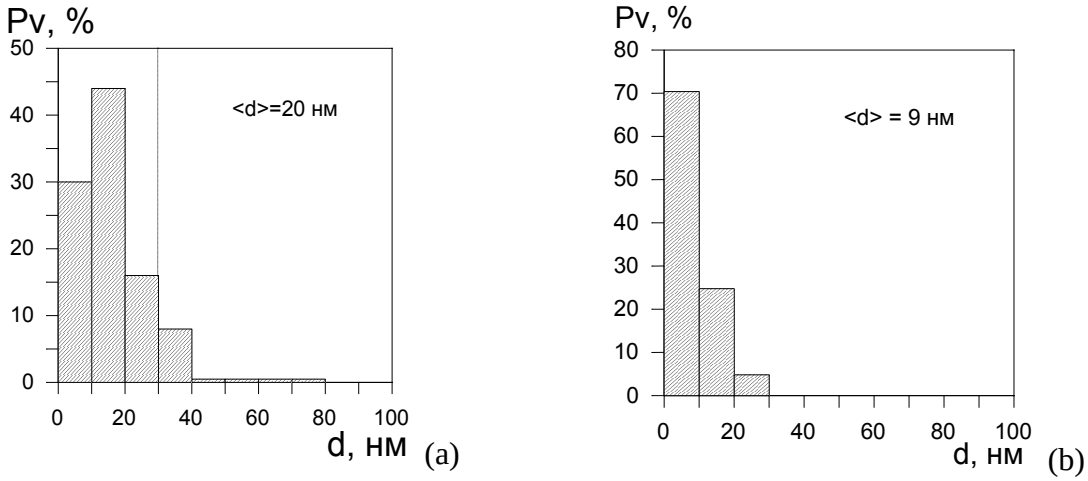

(a) (b)

Figure 2. Zirconia crystallite size distributions in initial ZrO_2 (3Y) and in ZrO_2 (3Y) + 20 wt. % Al_2O_2 powders (*a* and *b*, respectively)

The crystallite size for all nanocrystalline powder particles of the ternary system under investigation is ≤ 30 nm, which is below the critical value. This means that for a phase composition of zirconia in the particles being consistent with the critical-size concepts, no reflections of the *m* modification may be observed in the electron diffraction patterns. The foregoing electron diffraction data substantiate this conclusion and are evidence of the fact that the critical zirconia crystallite size in the nanocrystalline particles is no less than 30 nm.

Thus, the TEM data suggest that ZrO_2 (3Y) particles transparent to the incident electron beam have a nanocrystalline structure made up of zirconia grains. The majority of crystallites in ZrO_2 (3Y) are single-domain particles of high-temperature modifications. Reflections of the *m* modifications are seen solely in the electron diffraction patterns of particles made up of coarse grains.

In ZrO_2 (3Y) + 20wt. % Al_2O_3, there are both crystalline and quasi-amorphous particles. X-ray spectral microanalysis shows the presence of alumina in particles of the two kinds, with the alumina content in the particles approaching its total amount in the powder (20 wt %). The structure of the nanocrystalline particles in this powder is similar to that found in the binary system with nearly the same crystallite size. Judging by the electron diffraction data and those obtained by x-ray spectral microanalysis, the crystalline structure of the quasi-amorphous particles appears to correspond to a nonequilibrium solid solution based on high–temperature zirconia modifications with alumina addition.

3.2. Variations of the t-lattice microdistortions and coherently diffracting domain size in ZrO_2 (3Y)

Treatment and annealing of ZrO_2 (3Y) produced by plasma spray synthesis enable us to form a large number of *t* states with varying CDD average size and varying microdistortion level. Figure 3 is a plot of the microdistortion level against the CDD average size constructed with the use of data on the initial state and those obtained for the powder subjected to different type of treatment and annealing. For the CDD size lying in the range from 20 to 40 nm, the microdistortions increase with decrease in *D*. In the case where the CDD size is above 40 nm, the microdistortion level remains virtually constant ($\varepsilon_0 = 0.7 \cdot 10^{-3}$). Also shown in the figure is the microdistortion level ε_1 for ZrO_2 (3Y) in the initial state.

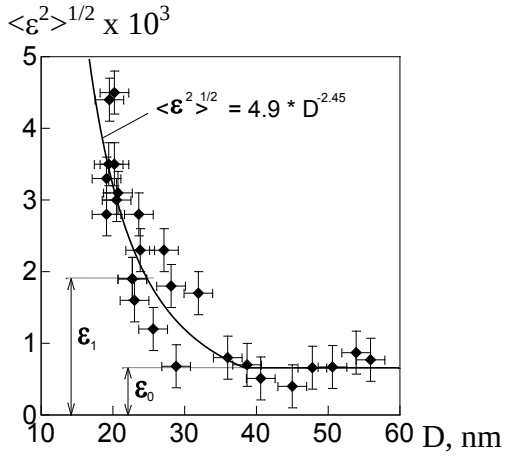

Figure 3. Lattice microdistortions versus CDD average size for nanocrystalline *t*-ZrO_2 (3Y) powder

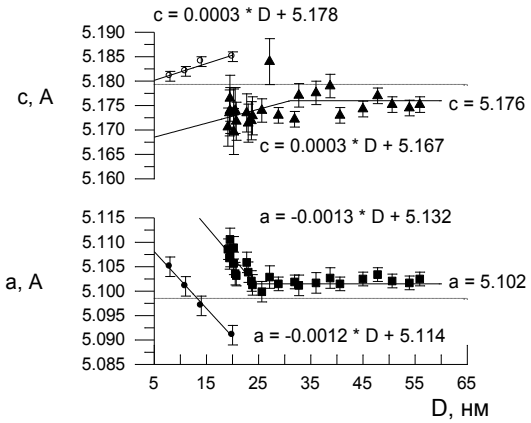

Figure 4. Tetragonal lattice parameters versus CDD average size for nanocrystalline *t*-ZrO_2 (3Y)

It is probable that the residual microdistortion level observed in *t*-ZrO_2 (3Y) for $D > 40$ nm (i.e., in the region where the grain boundary contribution is at a minimum) is primarily associated with defects of the inner regions of the crystal lattice. These are most likely to be point defects due to annealing like Y^{3+} ions of a larger ionic crystal radius than that of Zr^{4+} ions and oxygen lattice vacancies due to charge neutralization.

The increase in the microdistortion level with reduction of the CDD size down to < 40 nm testifies that the CDD size is limited by defects concentrated at the CDD boundaries. This is also demonstrated by the fact that the CDD average size in the powder material under study is in good agreement with the crystallite size, as revealed by TEM.

In the case where all microdistortions are due to interfaces, the following relation should be imposed: $\varepsilon \sim D^{-1}$. As is seen from Fig.3, the microdistortion level in the material under study for a CDD size of < 40 nm is increased in proportion to $D^{-2.45}$, i.e., the microdistortion accumulation rate is much higher in this case. Notably, the data for this relationship correspond for the most part to the *t*-

phase state after treatment. This behavior of the material appears to demonstrate that the increase in the microdistortion level occurs not only due to distortions of the subsurface crystallite layer, but due to an accumulation of lattice defects in the bulk of the crystallites as well. Hence, defects may be cation vacancies and interstitial Zr^{4+} and O^{2-} ions.

The *t* phase in ZrO_2 (Y) produced by plasma spray sintering is characterized by reduced tetragonality as compared to the coarse-grained material. A set of the *t*-phase states with varying CDD size obtained as the result of treatment and annealing enables us to examine the CDD size dependence of the lattice parameters. Figure 4 depicts *t*-lattice parameters as functions of the CDD average size for the powders under consideration. The *t*-lattice parameters reported in [7,8] for unstabilized powders of ZrO_2 produced by plasmochemical techniques are given for comparison. The dotted horizontal lines represent lattice parameters for a coarse-grained material of the ZrO_2 (Y) composition [9]. The lattice parameters are seen to exhibit regular changes for a CDD size of < 25 nm as compared to the unstabilized material. This appears to be due to a dissolved yttria effect. It is evident from the figure that in the ZrO_2 (3Y) powders under consideration, the lattice parameters approach each other for a CDD size of < 25 nm. For the CDDs of size > 25 nm, the two *t*-phase parameters in the stabilized material are no longer varied.

The fact that the ZrO_2 (3 Y) powders under study have close *t*-phase parameters for a CDD size of < 25 nm correlates well with the changes in the lattice parameters in unstabilized ZrO_2 as the CDD size is reduced from 20 down to 8 nm (Fig.4). This means that the lattice parameters of the powders produced by plasma spray synthesis for our experiments do change due to the CDD size effect. The slopes Δa and Δc of the curves representing the linear relationships between the parameters *a* and *c* for ZrO_2 (3Y) used in our investigations approach those observed in the unstabilized material. This suggests that similar mechanisms responsible for the *t*-lattice parameter variations with CDD size are involved in the two types of materials.

It should be noted that while the lattice parameters of the powders under consideration do vary with increase in the CDD size to > 25 nm, they do not reach the level characteristic of the coarse grained material (Fig.4). For $D > 25$ nm, their values correspond to those found in as-annealed powders. The behavior of the nanocrystalline *t*-phase parameters observed for $D > 25$ nm may be attributed to the presence of residual stresses in the crystallite structure. In this case, even annealing fails to provide complete stress relaxation. The residual stresses appear to favor the *m* to *t* transformation on annealing.

The set of the *t*-phase states of the powders also enables us to examine the correlation between the amount of the *m* modification in the material, on the one hand, and the average CDD size and lattice microdistortion level, on the other. Figure 5 shows variations of the *m*-phase abundance in ZrO_2 (3Y) with the CDD average size (*a*) and with *t*-lattice microdistortion level (*b*). Normally, the *m*-phase abundance is increased with increase in the average crystallite size. As is seen in Fig.5, this relation breaks down for $D = 20–60$ nm in the powders under consideration: as the CDD average size is increased, the *m*-phase abundance is decreased down to the point that the reverse (*m*–*t*) transformation takes place. The decrease in the *m* content with increase in the CDD average size for $D > 23$ nm testifies that the critical size approaches the characteristic values for sintered material (500–1000 nm). This fact substantiates our conclusion that grain boundaries become more perfect on annealing (i.e., annealing decreases the number of defects).

Inspection of Fig.5*b* discloses that the *m*-phase abundance, on the contrary, correlates closely with lattice microdistortions. This means that the increase in the *m* content for small values of *D* (Fig.5*a*) is really due to the microdistortion effect on the critical size, thus lending credence to the proposition that the phase composition of nanocrystalline zirconia is governed by *t*-lattice microdistortions.

Thus, the *t* phase in ZrO_2 (3Y) produced by plasma spray sintering exhibits variations of the lattice parameters due to the crystallite size. Unlike the coarse-grained material, the variations of the *t*-ZrO_2 (3Y) content are observed for a CDD average size of < 25 nm, with the *t*-phase structure approaching that of the *c* phase. For a CDD average size of < 40 nm, elastic straining of crystallite regions in the vicinity of grain boundaries was observed as microdistortions in diffraction experiments. The phase composition of the material under study is really controlled by the microdistortion level.

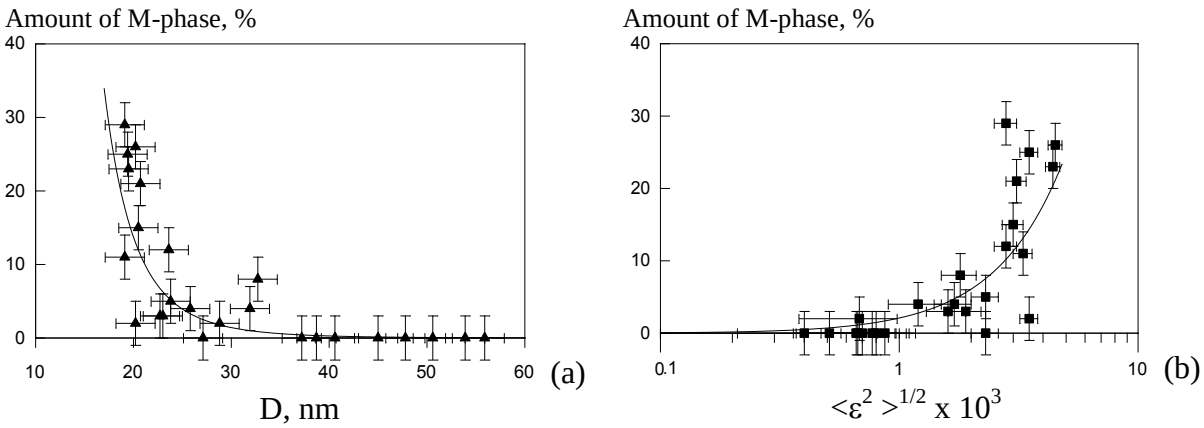

Figure 5. Variations of the amount of the *m* modification with CDD average size (*a*) and lattice microdistortions (*b*) in nanocrystalline *t*-ZrO_2 (3Y)

3. Porous structure and phase composition of ceramics

A porous structure of ceramics with porosity less than 10% mainly are the isolated pores. There are two types of porosity in ceramic with porosity 10 - 60%, those are isolated and continuous one, or the isolated pores and the porous clasters. The porous structure of ceramic with porosity more than 50% is a system of the continuous pores. One can observe the unimodal sizes distribution of pore, Fig. 6, the mean pore size being commensurable with the grain size. There appears the second peak in distribution in ceramic sintered with porophores: the first peak is defined by small pores, the presence of which is owing to packing of the initial powder particles, the second one is conditioned by the pores with configuration of porophores particles (Fig. 7), the greater portion of continuous porosity the greater mean pore size. As one can see in Fig. 8, the increasing volume of porosity decreases tetragonal phase content almost by 2 times. It is stipulated by the growing of crystallites and absence of compressive stresses in high-porous media, which stabilize the tetragonal phase.

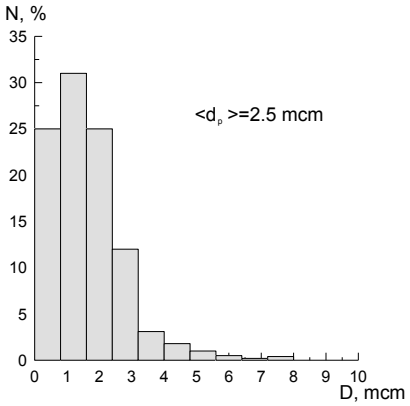

Figure 6. The size distribution of pores in ceramics with the mean size being commensurable with the grain size

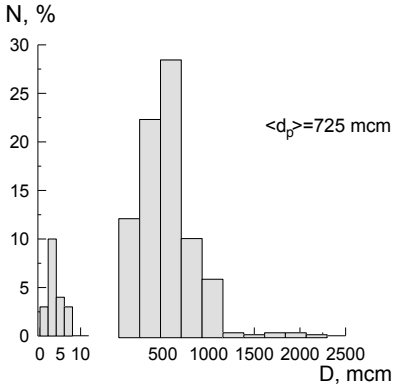

Figure 7. The size distribution of pores in ceramics with the mean size exceeding the grain size

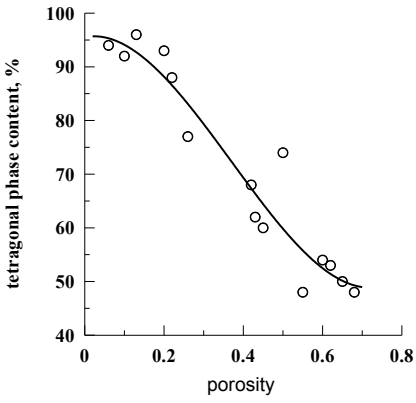

Fig ure8. The content of tetragonal phase in $ZrO_2(Y_2O_3)$ vs. porosity

4. Deformation behavior and mechanical properties of porous ceramics

The stress-strain curves for the ceramics with different porosity are shown that the material with porosity less than 10% has linear stress-strain curves with small deviation from linearity at the tip of a curve being apparently owing to t-m phase transition occurring under stresses, which is characteristic for partially stabilized ZrO_2 [3]. Ceramic with the higher porosity has the more complex curves. One can separate out some parts in curves. It is seen that the increase of the pore volume causes multiple microdamages during the deformation, which are the greater, the higher the porosity. In the curves, this process shows up as sharp stress drops due to microcracking. After the microcracks have terminated at the pores, the material can elastically deform again. As the porosity grows the range of microcracking shifts toward higher strains and

expands. When the porosity exceeds 20%, the stress-strain curves become concave upward, which is totally untypical of the stress-strain curves for sintered materials.

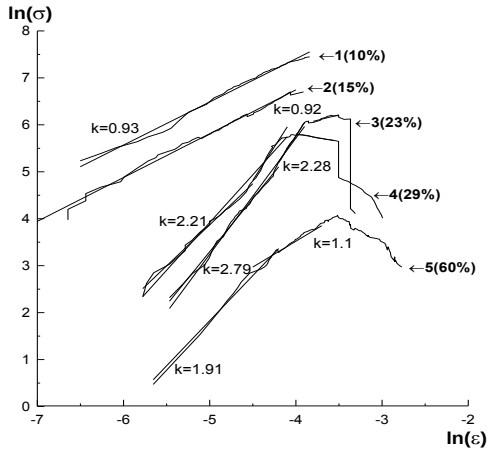

Figure 9. Stress-strain curves in log-log coordinates. Numbers is porosity

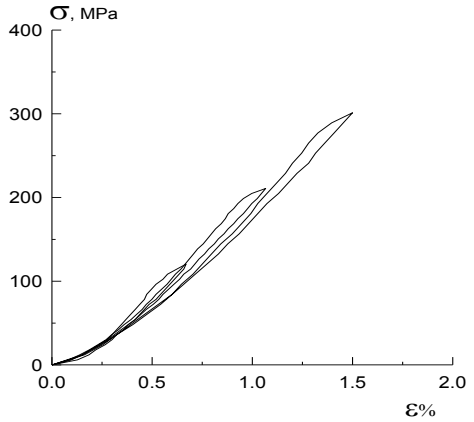

Figure 10 Stress-strain curves of ZrO_2 (Y_2O_3) under cycle

At the stage of high deformation (prior to microcracking), the general slope of the curves a **σ=f(ε)** varies with the porosity. However, the slope varies also locally (within one curve), depending on the porosity type and pore size. Such dependencies can be described by a power function like $\boldsymbol{Y=bX^k}$ for both deformation and pressing-related processes (the latter are also possible in this system). Here, the exponent ***k*** depends on which of the processes, pressing or plastic deformation is governing. For purely elastic deformation, k =1; for plastic deformation, $k < 1$; and for pressing, $k > 1$. In the most general case it is possible superposition of all the above mechanisms.

Figure 9 demonstrates the curves **σ=f(ε)** in the "log-log" coordinates. For the ceramic of porosity higher than 20%, the curves take the form of several linear segments, which obviously have various slopes *k*. The higher the porosity, the larger the number of the linear segments and all the values of k>1, with the highest values achieved for a number of materials, up to 2.5. So, it should be expected above all, there will be revealed pressing process, specifically under active deformation. In general, it is wonderful that there are k > 1 under deformation to small degrees, since it is impossible to find here the traces of fracture. For this purpose the special metallographic investigations has been carried out with specimens being exposed to deformation to small degrees, up to the very beginning of visual traces of fracture, and to cycle loading.

The examination of the sample surface after the deformation indicates no signs of local pressing - related material displacement before microcracking. Moreover, at this stage, the stress-strain curves are reversible, fig. 10, that is, the deformation process is purely elastic, as demonstrated by direct metallographic studies: there is no effect of irreversible displacement of the fragments into the porous space.

It is possible to determine the effective elastic modulus of system by the initial parts of the obtained deformation curves and the yield strength – by their maximum values. The value of the effective compressive modulus is known to depend on the porous space volume but it is insensible to pore configuration, whereas strength must depend on morphological structure of porosity owing to different curvature of its inner surface, for example. The dependencies of the yield strength and the effective compressive modulus on the porous space volume are illustrated in Figs. 11 and 12. As should be expected, the experimental results on strength are divided into two systems of points that is for high and low-level porosity, being arranged higher than in the case of microporous ceramics with the mean level porosity highly exceeding the grain size. The difference almost disappears with the porosity of ~ 60%. Modulus dependence on porosity is common for all the porosity types.

These strength and modulus dependencies on porosity are described by the equations as follows $Y=Y_o\exp(bX)$, which permit to determine strength and modulus of non-porous material. Their values well agree with the literature data, the coefficient **b** also correlating with the well-known values for similar materials.

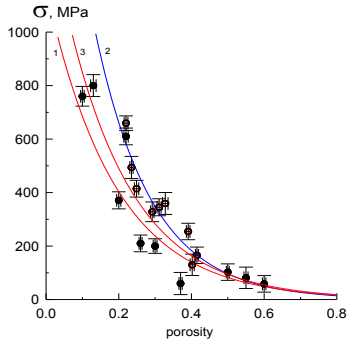

Figure 11. Strength of ZrO_2 (Y_2O_3) vs. porosity:
1. ceramics with pore size is comparable to the grain size, Y=1200exp(-5X);
2. ceramics pore size is much larger than the grain size, Y=2400exp(-6X);
3. averaging for all values, Y=1500exp (-5.5X)

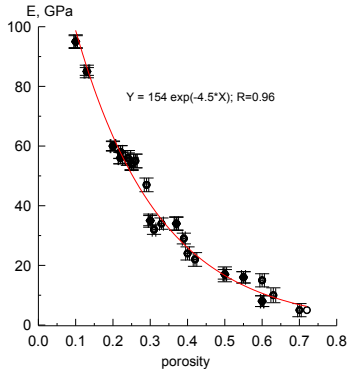

Figure 12. Effective elasticity modulus of ZrO_2 (Y_2O_3) vs. porosity

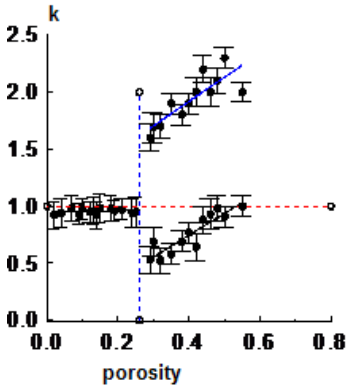

Figure 13. The parabolic factor **k** of the deformation equation vs. porous space volume of ZrO_2 (Y_2O_3) with pore size is comparable to the grain size

In Fig. 13, the exponents ***k*** measured from the slopes of the linear segments are plotted against porosity for the ceramic where the mean pore diameter is comparable to the mean grain size. The data points for ***k*** are well fitted by three straight lines. There exists some critical porosity value at which the deformation of the porous material radically changes: the second exponent of the power function (much larger than that in the initial state) appears. Most likely, this is related to a change in the pore distribution: individual pores give way to the continuous pore distribution. In essence, the material is split into two subsystems, which deform in different ways under stressing. It may be associated with change of pore distribution character from the isolated ones to the continuous porous structure.

As it was shown in [10], in this systems one can forms a linear or plate-like structures which admitting a model representation in the form of a rod, can exist in high-porosily ceramics with a limited area of contact between grains. Owing to a small size of the grains and the significant size of the contact area compared with the grain size and strong contact between grains formed during sintering, the bending stresses arising as a result of the loss of stability such rods do not exceed the ultimate strength of the ceramic material (which is virtually free of defects within the limits of the grain). That is there occurs the micromechanical instability of rod-like structures, obtained after sintering of porous body, with their considerable macro-deformation as structural elements, which may be realized in the elastic area as one can see from Fig.10.

5. Percolation transitions in porous ceramics

It should be assumed that qualitative changes occurring in ceramic macrostructure, namely the transition from the isolated pores to communicating porous structure, would be affected on the microstructural parameters. For this purpose, the coherent diffracting domain (CDD) sizes obtained from X–ray patterns have been plotted with the volume of ceramic porous space. These results are illustrated in Fig.14. As one can see, there takes place the increasing of CDD sizes with the increasing of ceramic porosity in the very beginning of a pattern; those being decreasing with the further increasing of porosity. With the increasing volume of porous space in the initial range (up to 15%) the increasing CDD size depend on diffusion growth of crystallites, which will be then controlled by stresses.

It is possible to find approximating by the dependencies like $F\sim(q-q_c)^m$, here m is the critical power index [11] and q_c is 0.15-0.17, that on the right and on the left from q_c both of the dependencies are put to the following form: $F_- \sim x^{5.3}$ and $F_+ \sim x^{5.9}$, which consequently, there are strong grounds to think that it is the correct interpretation of the obtained results in the terms of “the first percolation threshold” [11].

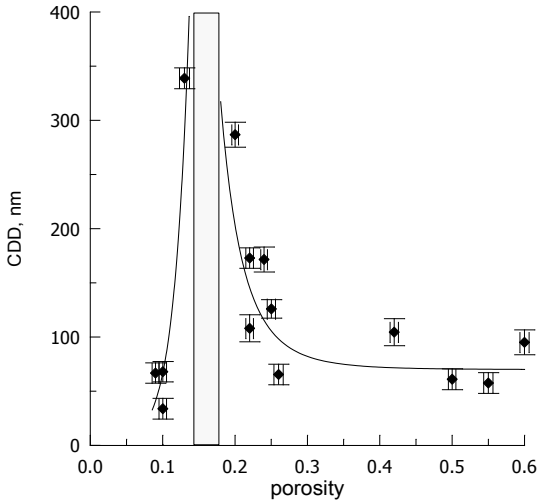

Figure 14. CDD-sizes vs. porosity

That is, in case of achieving some critical level of porosity, the basic changing character of the CDD dependence on porosity is associated with the percolation threshold in ceramics from the isolated pores to the continuous porous structure. The isolated pores do not qualitatively affect on the microstructural parameters, but in turn, the existing stresses restrict growth of the crystallites in the continuous porous ceramic structure.

4. Conclusion

1. Yttria and/or alumina-doped zirconia are in nanocrystalline and quasi-amorphous structural states. The nanocrystalline part of the material is in the *t*-phase state, while its quasi-amorphous part is in the *t*- or *c*-phase state. The crystal structure of the nanocrystalline and quasi-amorphous parts of the material is a nonequilibrium solid solution of ZrO_2(Y, Al). In the powder yttria stabilized with alumina addition, the *m* phase in ZrO_2 is formed due to increase in the microdistortion level which destabilizes the nanocrystalline *t* phase.
2. It was shown that in the porous structure of zirconia ceramics there is a critical value of porosity the material divides into two sub-systems, being variously deformable under external loading. There is no effect of irreversible displacement of the fragments into porous space.
3. In ceramics with the porosity up to 70% there occurs the micromechanical instability of rod-like structures, obtained after sintering of porous body, with their considerable macro-deformation as structural elements, which may be realized in the elastic area.
4. It has been found out the correlation between the sizes of crystallites and porosity, which associated with transition of the isolated porous structure to the continuous one and the porosity of 20%, corresponds to the first percolation threshold.

Acknowledgement
This work was partial financial supported by Tomsk State University Competitiveness Improvement Program and Siberian Branch Program #III.23.2.3.

5. References

[1] G.L.Messing, Shi-Chang Zang, and G.V.J-Ayanti, J.Amer.Ceram.Soc., **76**, No.11, 2707–2726 (1993)
[2] Porous Structural Ceramics. Ed. By Yu.Krasulin. (Metallurgia, Moscow, 1980)
[3] Evans A.G. J. Amer. Ceram. Soc, 1990. V.**73**, #2. Pp.187-206.
[4] G.K.Williamson and W.H.Hall, Acta Metall., **1**, 22–31 (1953).
[5] S.N.Kulkov, P.V.Korolev, A.G.Melnikov, *et al*., Russ. Phys. J., **38**, No.1, 42–45 (1995).
[6] Yu.F.Ivanov, V.V.Lopatin, and V.S.Dedov, Russ. Phys. J., **37**, No.1, 95–101 (1994).
[7] V.F.Petrunin, Zhur. Vsesoyuz Khimich. Obshch. Im. D.I.Mendeleev, **36**, No.2, 146–150 (1991).
[8] V.F.Petrunin, A.G.Ermolaev, A.V.Burkhanov, *et al*., Poroshk.Metallurg., No.**3**, 47–52 (1989).
[9] D. –J.Kim, J. Amer. Ceram. Soc., **73**, No.1, 115–120 (1990).
[10] Kulkov S., Maslovskii V. et al.Technical Physics, v.**47**, #3, 2002, pp.320-324.
[11] Sahimi M. Application of Percolation Theory. (L.: Taylor &Francis. 1994)